Journal of Catalysis 268 (2009) 356–366

Contents lists available at ScienceDirect

Journal of Catalysis

journal homepage: www.elsevier.com/locate/jcat

A green pathway for hydrogenations on ionic liquid-stabilized nanoparticles

Fabian Jutz, Jean-Michel Andanson, Alfons Baiker *

Institute for Chemical- and Bioengineering, Department of Chemistry and Applied Biosciences, ETH Zurich, Hönggerberg, HCI, CH-8093 Zurich, Switzerland

ARTICLE INFO

Article history:
Received 19 August 2009
Revised 5 October 2009
Accepted 6 October 2009
Available online 1 November 2009

Keywords:
Ionic liquids
Nanoparticles
Palladium
Rhodium
Supercritical CO_2
Acetophenone
Chemoselective hydrogenation
in situ IR spectroscopy
Green chemistry

ABSTRACT

Ionic liquid and supercritical carbon dioxide have been employed to facilitate a green pathway for solventless noble metal-catalyzed hydrogenations. The catalytic system consisted of *in situ*-synthesized palladium and rhodium nanoparticles stabilized by various ionic liquids ([BMIm][PF_6], [BMIm][OTf], and $N(C_6H_{13})_4Br$). Supercritical CO_2 extraction was employed for the removal of the metal precursor ligands in the catalyst synthesis step as well as for the separation of the hydrogenation products. All steps, including catalysts synthesis, reaction, and product separation, were followed by *in situ* infrared spectroscopy. The potential of this concept is shown using the example of the palladium- and rhodium-catalyzed hydrogenation of acetophenone. The most efficient catalyst, Pd-[BMIm][PF_6], exhibited good activity and excellent selectivity and showed no deactivation during multiple reaction cycles.

1. Introduction

The selective reduction of carbonyl compounds by means of heterogeneous catalysts is an important field in industrial organic chemistry [1]. Acetophenone (AP) serves as a particularly interesting substrate, as its hydrogenation pathway leads to several products and byproducts, mainly due to the competitive and consecutive hydrogenation of the carbonyl function and the aromatic ring (Scheme 1), thus offering an ideal model substrate for chemoselective hydrogenation reactions. One of the desired hydrogenation products is 1-phenylethanol (PE) which is used in pharmaceutical and fragrance industries [2]. Various heterogeneous catalytic systems are reported, employing Pd, Pt, Ni, Cu, Ti, or Ru catalysts at a wide range of pressures and temperatures, most of them consisting of "classical" supported noble metals in organic solvents [3–11].

Ionic liquids (IL) have gained remarkable interest in catalysis during the past years, mainly serving as "green" solvents due to their negligible vapor pressures or as support phase for supported ionic liquid phase (SILP) catalysis [12–22]. Especially in combination with supercritical CO_2, ionic liquids exhibit interesting properties in multiphasic catalytic reactions. Supercritical CO_2, otherwise being an excellent solvent for various substances, does not dissolve ionic liquids, whereas CO_2 is soluble in ILs and is able to extract substances out of them [23–30]. Furthermore, CO_2 is able to lower the melting point of ILs [31–33]. Additionally, CO_2 seems to decrease the viscosity of ionic liquids [24,34]. This combination offers convincing opportunities for a "green" process design, combining the outstanding solvent properties of supercritical CO_2 with the particular properties of ILs. Apart from their properties as support phase, ionic liquids are increasingly used to generate metal nanoparticles of defined size and shape. Also their ability to stabilize metal nanoparticles by forming a layer around them is reported by several groups, and those particles are successfully applied in various catalytic reactions [31,35–48].

The aim of this study was to investigate the performance of newly synthesized Pd and Rh nanoparticles in the chemoselective hydrogenation of acetophenone, while maintaining a complete "green" process by combining the facile additive-free synthesis of the catalyst with the hydrogenation reaction and a subsequent product extraction by supercritical CO_2, as illustrated in Scheme 2.

An important feature was to abstain from the use of conventional solvents while only using a small amount of ionic liquids to stabilize the nanoparticles. Another goal was to perform several reaction/extraction cycles and thus investigating also the reusability of the most promising catalyst. FTIR spectroscopy proved to be a very useful tool to study *in situ* the selectivity and the kinetics of this reaction [49] and to follow on line the CO_2 extraction process. Two different metals and three different ionic liquids were used to synthesize nanoparticles which were successfully employed as catalysts for the solventless chemoselective hydrogenation of acetophenone.

* Corresponding author. Fax: +41 44 632 1163.
E-mail address: baiker@chem.ethz.ch (A. Baiker).

0021-9517/$ - see front matter © 2009 Elsevier Inc. All rights reserved.
doi:10.1016/j.jcat.2009.10.006

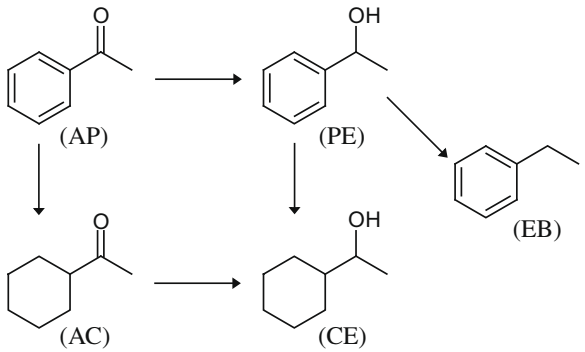

Scheme 1. Overview on the hydrogenation pathways of acetophenone (AP). The possible products include 1-phenylethanol (PE), ethylbenzene (EB), acetylcyclohexane (AC), and 1-cyclohexylethanol (CE).

2. Experimental

2.1. Materials

For the synthesis of the nanoparticles, the metal precursors $Rh(OAc)_3$ (rhodium(III) acetate, 99.9%, ABCR), $Rh(acac)_3$ (rhodium(III) acetylacetonate, >99%, ABCR), and $Pd(acac)_2$ (palladium(II) acetylacetonate, >99%, Acros Organics) were used as obtained. The employed ionic liquids [BMIm][PF_6] (1-*n*-butyl-3-methylimidazolium hexafluorophosphate, 98% (Cl^- < 10 ppm), ABCR), [BMIm][OTf] (1-*n*-butyl-3-methylimidazolium trifluoromethanesulfonate, 99% (Cl^- = 10 ppm), Alfa Aesar), and $N(C_6H_{13})_4Br$ (tetrahexylammonium bromide, >99%, Fluka) were taken from freshly opened bottles without further purification. H_2 (99.995%) and CO_2 (99.9%) were supplied by PanGas. Hexane (96%, Scharlau) and cyclohexylcyclohexane (>99%, Fluka), employed for GC-analysis of the products, were also used as received.

2.2. Synthesis of the nanoparticles

All nanoparticles were synthesized in a 60 mL stainless steel (316 L) autoclave (Premex, Switzerland) equipped with an active heating system and a magnetic-coupled paddle stirrer. The subsequent supercritical CO_2 extraction of the precursor ligand and other impurities was performed in a continuous extraction unit (NWA PE-310), containing a 300 mL stainless steel (316Ti) autoclave, equipped with an active heating system and a magnetic-coupled paddle stirrer.

2.2.1. Synthesis of Pd–$N(C_6H_{13})_4Br$

$N(C_6H_{13})_4Br$ of 1.01 g (2.32 mmol) were mixed carefully with 64.3 mg (0.21 mmol) $Pd(acac)_2$ directly in the autoclave. After closing, the autoclave was flushed with hydrogen and adjusted to a hydrogen pressure of 50 bar. Heating was set to 110 °C in order to melt the ionic liquid and ensure a homogeneous mixing. The stirrer was set to 200 rpm and the mixture was left for 3 h. After cooling and depressurizing, a gray glassy solid was obtained, which was transferred into the extraction autoclave and extracted for 5 h. The extraction process was performed under a constant CO_2 pressure of 100 bar and at a temperature of 60 °C. After the extraction, the obtained gray glassy material was ground into a powder.

2.2.2. Synthesis of Rh–$N(C_6H_{13})_4Br$

$N(C_6H_{13})_4Br$ of 1.00 g (2.30 mmol) were carefully mixed with 89.0 mg (0.89 mmol) $Rh(acac)_3$ and treated exactly the same way as described in Section 2.2.1. After extraction, a dark, brownish gray glassy material was obtained which was ground into a powder.

2.2.3. Synthesis of Pd–[BMIm][PF_6]

[BMIm][PF_6] of 3.01 g (10.6 mmol) were placed in the autoclave, followed by the addition of 0.252 g (0.83 mmol) $Pd(acac)_2$. The mixture was carefully stirred with a spatula, until a homogeneously mixed yellow suspension was obtained. The autoclave was then closed, flushed with hydrogen, and adjusted to a hydrogen pressure of 14 bar. Under moderate stirring (200 rpm) the reactor was slowly heated to 50 °C and left for 4 h. After that, the reactor was cooled down, opened, and the obtained black viscous mixture was transferred into the extraction autoclave. The extraction process was performed at a constant pressure of 100 bar and a temperature of 55 °C to ensure supercritical conditions for 6 h. A thoroughly black homogeneous mixture was obtained.

2.2.4. Synthesis of Rh–[BMIm][PF_6]

[BMIm][PF_6] of 1.396 g (4.91 mmol) were placed in the autoclave, followed by the addition of 0.216 g (0.77 mmol) $Rh(OAc)_3$. The subsequent procedure was identical to the one described in Section 2.2.3., the only difference being a longer hydrogenation time of 8 h instead of 4 h. After extraction, a homogeneously black viscous mixture was obtained.

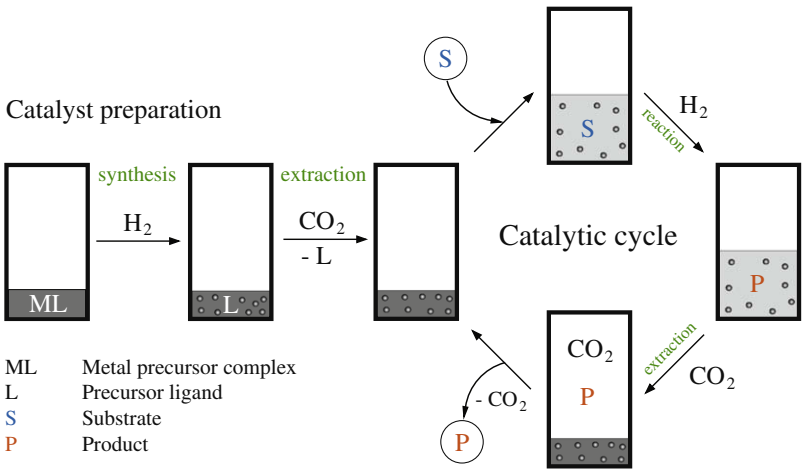

Scheme 2. Schematic view of the complete "green" pathway. The catalyst preparation step consists of the formation of the nanoparticles in the ionic liquid, followed by supercritical CO_2 extraction of the precursor ligand. In the catalytic cycle the hydrogenation reaction is followed by supercritical CO_2 extraction of the product, after which new substrate can be added to restart the cycle.

2.2.5. Synthesis of Pd–[BMIm][OTf]

[BMIm][OTf] of 7.01 g (24.3 mmol) were filled in the autoclave and 0.24 g (0.79 mmol) $Pd(acac)_2$ were added. The complete synthesis and extraction procedure was performed according to Section 2.2.3., yielding a black viscous liquid.

2.3. Catalyst characterization

In order to ensure that the precursor ligand was completely removed during the extraction process, all catalyst materials obtained were analyzed by ATR-IR (attenuated total reflection infrared) spectroscopy in a BRUKER EQUINOX 55 spectrometer equipped with a liquid nitrogen-cooled mercury cadmium telluride (MCT) detector and holding a trapezoidal ZnSe crystal (50 × 20 × 2 mm, angle of incidence 60°) as internal reflection element. No signals except the ionic liquid bands were detected.

Transmission electron microscopy (TEM) measurements were performed on a CM30ST microscope (Philips; LaB_6 cathode, operated at 300 kV, point resolution ~2Å). The particles were dispersed in acetone and deposited onto a perforated carbon foil supported on a copper grid. The microscope was also equipped with a high angle annular dark-field (HAADF) detector for scanning transmission electron microscopy showing the metal particles with bright contrast (Z contrast). Where applicable, the mean metal particle size was calculated based on a minimum of 250 particles.

2.4. In situ IR measurements and kinetic studies

In situ infrared spectroscopy measurements, especially for monitoring the reaction progress under various conditions and for following the extraction process, were performed in a high pressure view cell with variable volume and several optical probing paths. The cell is equipped with two sapphire windows to observe the phase behavior and two ZnSe windows for transmission IR measurements of the gas phase. Additionally, the cell contains an ATR-IR ZnSe crystal on the bottom to investigate the liquid phase. Other details of the cell are described elsewhere [50]. Infrared spectra were measured with an IFS-66 spectrometer (Bruker Optics) with a resolution of 2 cm^{-1} in the range of 4000–600 cm^{-1} for ATR-IR measurements and 8000–600 cm^{-1} in transmission mode.

In a typical hydrogenation experiment, a defined amount of catalyst suspension was carefully filled into the cavity above the ATR crystal, followed by the addition of a known amount of substrate (AP) and a magnetic stirring bar. The cell was flushed with hydrogen and afterwards pressurized to the desired pressure of the experiment. If required, the cell was heated to the desired temperature. Spectra were taken every 10 min until the reaction was complete.

The extraction process by supercritical CO_2 was initiated by releasing the hydrogen pressure and introducing CO_2 by means of a compressor (NWA PM-101). If this step was following an experiment at room temperature, the cell was first heated to 40 °C in order to be above the critical temperature of CO_2 (31.1 °C). Transmission IR spectra were recorded repeatedly to observe the evolution of the product bands being extracted from the ionic liquid phase. The most prominent bands reached saturation within seconds. CO_2 was then slowly released from the cell while introducing new CO_2 from the compressor, thus establishing a continuous extraction process while carefully maintaining a pressure above 90 bar within the cell. *Note that the release valve had to be heated during this process in order to prevent potentially dangerous freezing.* The transmission IR spectra indicated a complete extraction and removal from the cell within 10 min. A following ATR-IR measurement of the ionic liquid phase confirmed the successful extraction. The cell was then depressurized and opened. For the recycle experiments, a new substrate was introduced without further treatment of the catalyst and the catalytic experiment was restarted.

The ATR-IR spectra obtained with these experiments were analyzed by a deconvolution method and fitted with Gnuplot 4.2 software. A detailed description of this method is given elsewhere [49]. The *in situ* IR measurements and the following analysis of the spectra allowed the extraction of valuable information such as reaction kinetics and the influence of pressure and temperature on the reaction progress and the concentration of the products and the reactant.

2.5. Hydrogenation reactions

In order to further study the reaction parameters and to reproduce the results obtained by *in situ* measurements, conventional batch reactor experiments were performed. Three parallel stainless steel (316 L) autoclaves (Premex, Switzerland) with an individual volume of 50 mL were employed. The reactors are equipped with a heating jacket and an internal thermocouple. Stirring was performed by the addition of a magnetic stirring bar, which was operated by a magnetic stirring plate on which the reactors were placed.

In a typical experiment, a defined amount of catalyst suspension was filled into the autoclave, followed by the addition of a known amount of substrate (AP). The magnetic stirring bar was introduced and the autoclave was closed. After that, the reactor was flushed with hydrogen and then pressurized to the desired hydrogen pressure. At the end of the experiment, the pressure was released and the reactor was opened. Immediately a defined amount of internal standard (cyclohexylcyclohexane) was added and the contents of the reactor were collected and analyzed by gas chromatography (GC). For the GC measurements, a gas chromatograph (Thermoquest Trace GC, CE Instruments) equipped with a HP-FFAP capillary column (30 m × 0.32 mm × 0.25 μm) was employed. Turnover frequencies (TOFs) reported here were calculated based on the total metal content, and not on the number of surface atoms, and are therefore conservative estimates.

Safety note

The experiments described in this paper involve the use of high pressure and require equipment with an appropriate pressure rating and safety mechanisms.

3. Results

3.1. Synthesis of the nanoparticles

3.1.1. Particles synthesized in $N(C_6H_{13})_4Br$

TEM pictures and histograms depicting the particle size distribution of the alkylammonium bromide-based catalysts are presented in Fig. 1. Both Pd and Rh nanoparticles show a narrow size distribution of 3.5 ± 0.6 nm and 2.8 ± 0.7 nm, respectively. The metal loading of 2.25% in mass for Pd and 2.29% for Rh is comparable; however, a significant difference in particle size and also in particle dispersion is observable. The obtained solid catalyst materials with melting points just below 100 °C showed very similar macroscopic properties, with slightly different gray color.

3.1.2. Particles synthesized in [BMIm][PF_6] and [BMIm][OTf]

The ionic liquids containing a 1-*n*-butyl-3-methylimidazolium cation are the so-called colorless room temperature ionic liquids (RTILs) with high viscosity. The catalysts synthesized in these ionic

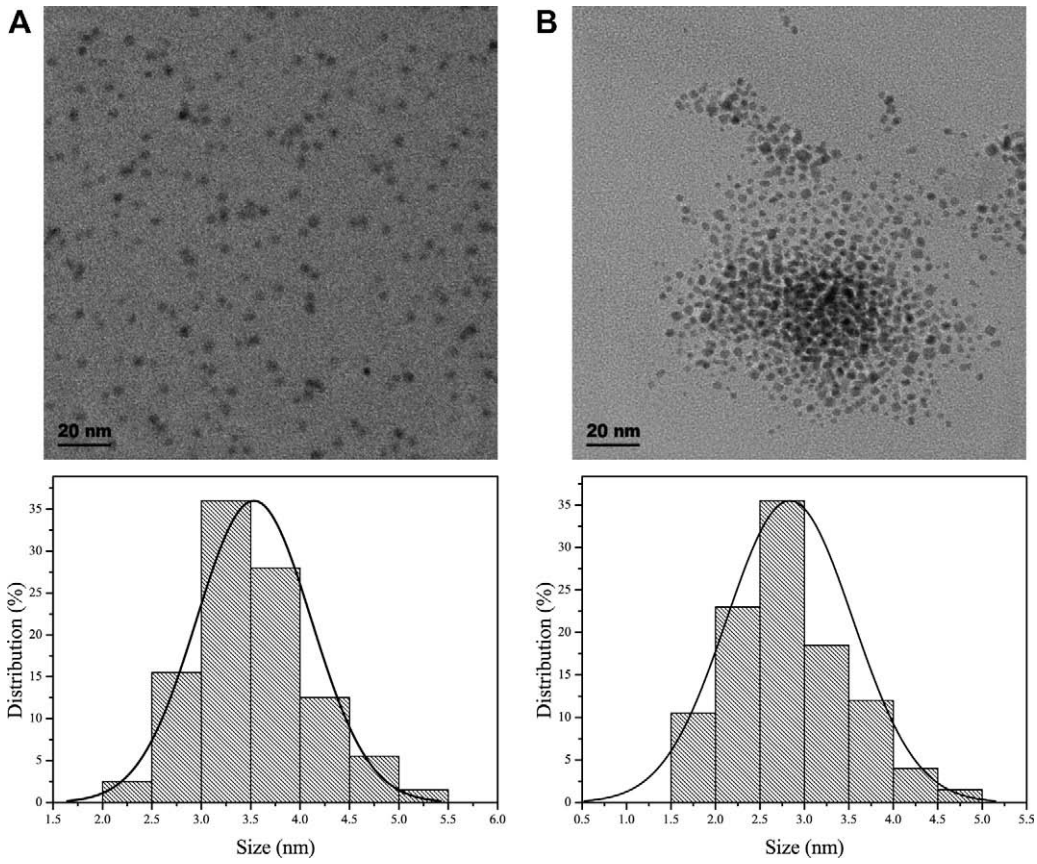

Fig. 1. TEM images of (A) Pd nanoparticles stabilized by $N(C_6H_{13})_4Br$ and (B) Rh nanoparticles stabilized by $N(C_6H_{13})_4Br$. The corresponding size distribution histograms are shown below the TEM images.

liquids showed a tendency to phase separation after a storage time of several days, as a black layer was formed on the bottom of the container flask and the overlying ionic liquid layer underwent continuous decoloration. This tendency was stronger for the Pd-based catalysts, especially for the catalyst synthesized in [BMIm][OTf]. However, after short shaking the suspensions turned completely black again and remained in this state as freshly synthesized. TEM images and electron diffraction patterns of all three catalysts synthesized in the RTILs are presented in Fig. 2. In all cases, the TEM images show a trend toward agglomeration of the particles. This effect was least prominent in the Rh nanoparticle suspension, where clearly separate yet agglomerated particles of 5–10 nm were observed (Fig. 2, bottom row). The Pd particles in the same ionic liquid exhibited a stronger agglomeration and the formation of significantly bigger structures with a diameter of 10–30 nm (Fig. 2, middle row). In the enlarged image (Fig. 2, E), a layer of organic substance surrounding the metal is visible, which probably can be attributed to [BMIm][PF_6]. In the case of Pd–[BMIm][OTf], a similarly strong agglomeration was observed (Fig. 2, top row). The diameter of these structures is in the same range as in the other ionic liquid, but the morphological details are considerably different. While in [BMIm][PF_6] mainly round-shaped metal nanoparticles were obtained, the fine structures in [BMIm][OTf] exhibited a more needle-shaped, dendrite-type of morphology (Fig. 2, B). Also the organic layer observed in the other case was not as clearly visible in these images. The electron diffraction patterns however showed very similar characteristics for both Pd samples, with identical line features (Fig. 2, C and F). The Rh electron diffractogram contained the same line features, but a slightly less ordered crystallinity (Fig. 2, I).

3.2. Hydrogenation reactions

3.2.1. Hydrogenation reactions with Pd nanoparticles

The results of the hydrogenation reactions catalyzed by Pd nanoparticles are summarized in Table 1. Freshly synthesized Pd–[BMIm][PF_6] showed a good performance with almost complete conversion after 4 h and a selectivity of nearly 90% at room temperature and 50 bar H_2 (entry 1). After storage and exposition to air for 3 months however the selectivity dropped by almost 5%, while an increasing formation of the hydrogenolysis product ethylbenzene (EB) was observed (entry 2). This effect was attributed to the formation of traces of hydrofluoric acid and is addressed in more detail in Section 4.3. The drop in selectivity for the somewhat aged catalyst could be completely reversed by repeating the supercritical CO_2 extraction step. After this, both selectivity and conversion were higher than 93% (entry 3), thus a complete regeneration of the catalyst was achieved. The selectivity did not drop while the activity increased at a slightly higher temperature of 40 °C, which is required when an immediate subsequent extraction by supercritical CO_2 is performed (entry 4). A further rise in reaction temperature to 50 °C however led to a decrease in selectivity, even for freshly extracted catalyst material (entry 5). Lowering the hydrogen pressure to 10 bar at 50 °C reaction temperature resulted in a further decrease in selectivity which reached values below 70% (entry 6). The highest selectivity of 99.8% with this catalyst was obtained when the reaction was stopped after 2 h with only 42.1% conversion (entry 7), as the main side product EB is a subsequent product of PE and mainly formed in later stages of the reaction.

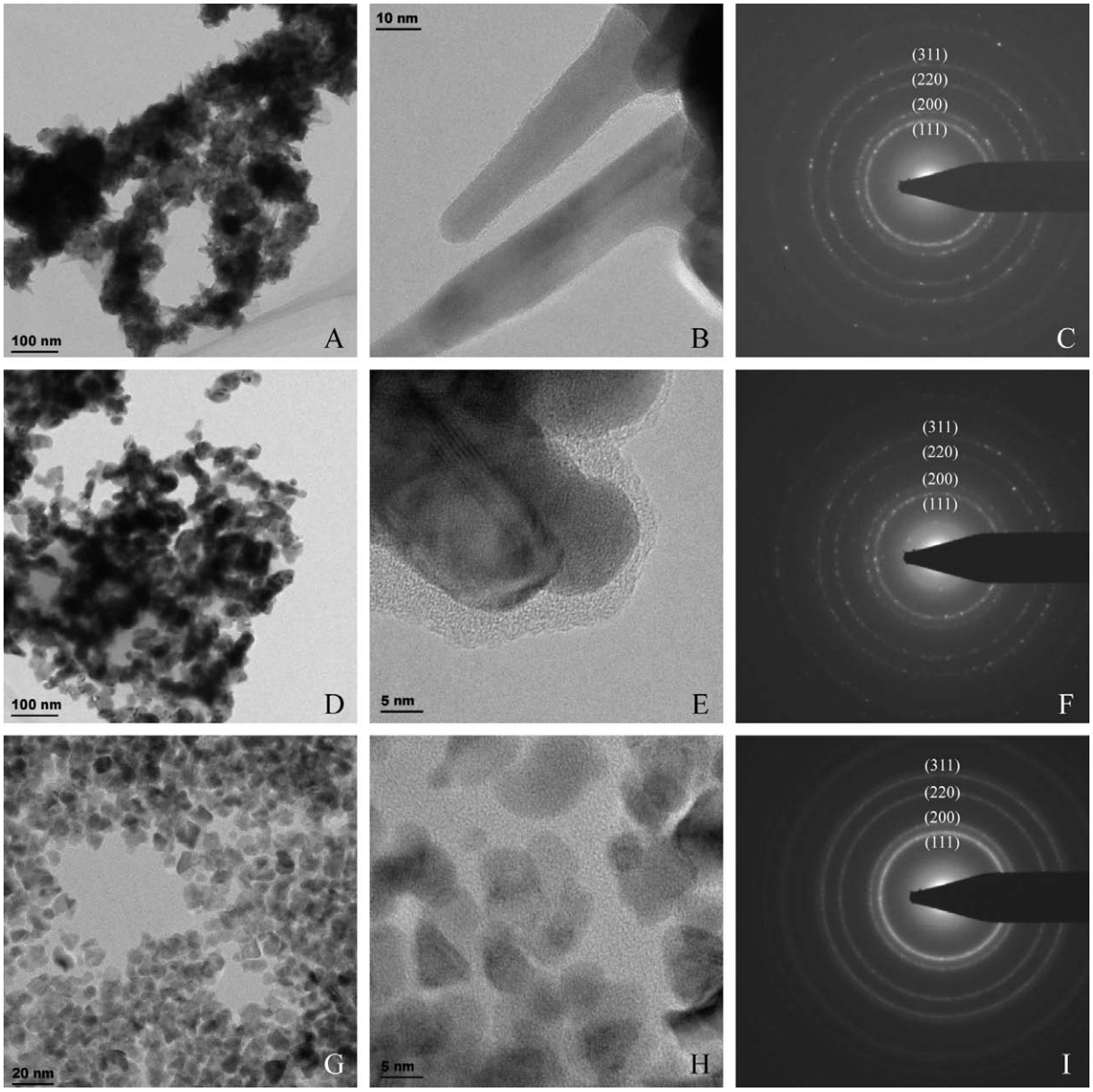

Fig. 2. TEM images including detail views of (A and B) Pd–[BMIm][OTf]. (D and E) Pd–[BMIm][PF_6], and (G and H) Rh–[BMIm][PF_6]. The electron diffraction patterns (C, F, and I) belong to the image sections on the same row.

The catalyst consisting of Pd–$N(C_6H_{13})_4Br$ showed virtually no catalytic activity for this reaction, with a conversion below 1% (entry 8) at room temperature and 50 bar. Although the solid material was dissolved in the substrate AP, also reactions above the melting point of $N(C_6H_{13})_4Br$ did not lead to increased activity.

Pd–[BMIm][OTf] exhibited relatively low catalytic activity compared to Pd–[BMIm][PF_6]. Activities expressed as turnover frequencies (TOFs) were always lower by a factor of 4–5. On the other hand, the former material showed excellent selectivity of nearly 100% at room temperature, obviously independent from the pressure which was varied between 15 and 100 bar (entries 9–11). However, the conversion in these reactions was comparably low. In order to reach useful conversions within reasonable time, a higher temperature of 60 °C was employed, which led to a satisfactory result of 96.6% conversion and 98% selectivity within 4 h.

3.2.2. Hydrogenation reactions with Rh nanoparticles

The results of the hydrogenation reactions with Rh nanoparticles are presented in Table 2. Overall, the selectivity toward PE was significantly lower than that in the reactions catalyzed by Pd. In all cases, significant aromatic ring hydrogenation occurred, while the hydrogenolysis byproduct EB was only observed in traces. This is in strong contrast to the products formed with Pd, where generally only PE and EB were found (for a detailed list of the products obtained in the reactions reported here, see Supplementary Material). As the TOF values indicate, the activity of Rh–[BMIm][PF_6] was lower by a factor of 2 compared to that of the analogue Pd catalyst. Higher reaction temperature led to higher conversion but lower selectivity under otherwise identical conditions (entries 1 and 9), as 41.4% conversion and 69.5% selectivity were reached at room temperature, while 73.6% conversion and 56.9% selectivity were obtained at 80 °C. The effect of pressure on the outcome of the reaction with otherwise identical parameters (entries 9 and 10) resulted in no observable rate enhancement (73.6% and 72.3% conversion at 10 bar and 50 bar, respectively), but the selectivity dropped drastically from 56.9% in the low pressure experiment to 37.6% in the high pressure experiment. The same effect was observed in the room temperature experiments

(entries 1 and 2). The twice as long reaction time lowered the selectivity toward PE because PE tends to be further hydrogenated to the saturated side product cyclohexylethanol (CE) with longer reaction time. Interestingly, this pressure effect was reversed at 40 °C, when both conversion and selectivity rose between 10 and 50 bar under otherwise identical conditions (entries 5 and 6). Also the experiment with 100 bar and 40 °C (entry 8) showed a higher selectivity than the experiment at 10 bar and the same temperature (entry 5). As the reaction time was longer, however, the selectivity was lower than that at 50 bar (entry 6). Another trend was observed when the catalyst amount was varied. With roughly double the catalyst amount and otherwise identical conditions, almost full conversion was reached at room temperature and 50 bar, while with half of that catalyst amount only 77.8% was obtained (entries 3 and 4). At the same time the selectivity dropped from 48.5% to 41.3%. Again, at 40 °C this effect was reversed. Doubling the catalyst amount led to an expected increase in conversion from 34.5% to 39.5% (entries 6 and 7), but surprisingly the selectivity also rose from 65.0% to 89.2%.

Unlike the analogue Pd catalyst, also Rh–$N(C_6H_{13})_4Br$ showed good performance, exceeding Rh–[BMIm][PF_6] and even the Pd catalysts in terms of activity, exhibiting a TOF of 38.7 h^{-1} (entry 11). However, the selectivity appeared with 42.2% comparably low, and a lower AP/Rh ratio could not be achieved under solventless conditions, as the solubility of high amounts of the solid catalyst in AP is limited.

3.3. In situ ATR-IR experiments

The progress of the reaction for both Pd- and Rh–[BMIm][PF_6] was studied by means of *in situ* ATR-IR spectroscopy. Direct spectroscopic observation of the ionic liquid phase allowed on line monitoring of the reaction progress and discrimination of the concentration of the different hydrogenation products. The spectra of a complete reaction catalyzed by Pd–[BMIm][PF_6] at 25 °C and 50 bar are depicted in Fig. 3. All spectra shown were recorded with an interval of 20 min, except for the last one which was recorded 720 min after the previous, illustrating the complete reaction after an overnight experiment. The spectra on the top show the lower wavenumber region between 800 and 1800 cm^{-1}, where the continuous disappearance of the AP bands is clearly visible. These bands, including the C=O stretching mode of AP located around 1700 cm^{-1}, are suitable to calculate the conversion. Product bands, mainly from PE, are comparably small in this region and in several cases overlapping with ionic liquid bands, thus not being suitable for product quantification. The spectra on the bottom, ranging from 2700 to 3600 cm^{-1}, mainly show the C–H stretching mode region and the O–H bands. The chronologic development clearly shows an increase of the broad OH band above 3200 cm^{-1}, which is a clear indicator for the formation of alcohols (in this case PE) by hydrogenation of AP. The changes in the CH region around 3000 cm^{-1} can be attributed to the formation of the cyclohexyl group of both PE and EB, the latter being formed in more advanced stages of the reaction, which is visible, e.g. in the band slightly above 2900 cm^{-1}.

A multivariate analysis of the spectra allowed the extraction of concentration profiles of the individual products, which helped analyzing the reaction kinetics. The details of this analysis, focusing on the less selective reaction with Rh–[BMIm][PF_6] are reported elsewhere [49]. Typical examples of thus obtained kinetic profiles are depicted in Fig. 4. As visible from the figure, Rh–[BMIm][PF_6] was much less active than Pd–[BMIm][PF_6], although both pressure and temperature were significantly higher. Regarding the selectivity, Rh showed a complex hydrogenation pathway with C=O hydrogenation and competitive aromatic ring hydrogenation. At the beginning of the reaction, PE was formed

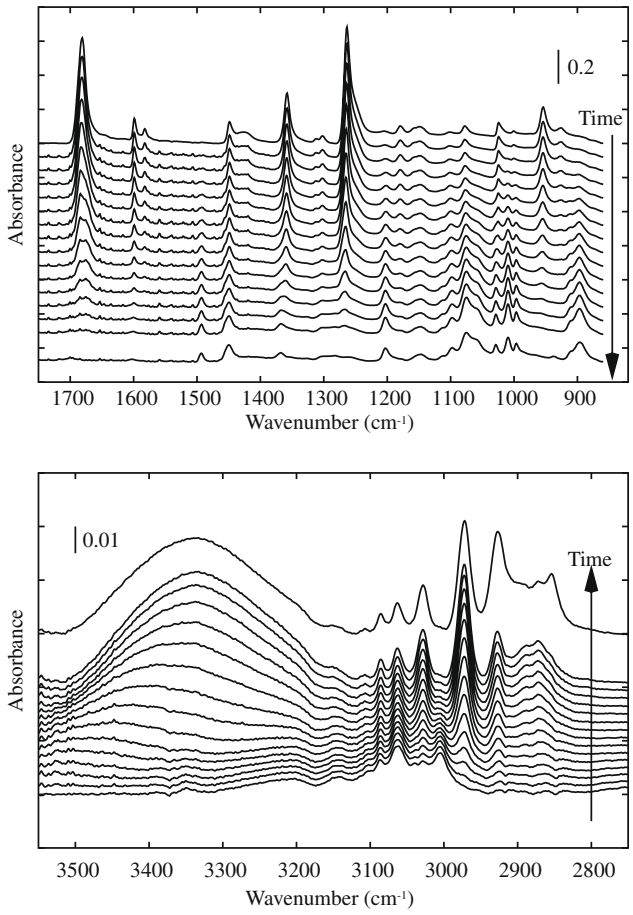

Fig. 3. *In situ* ATR-IR spectra of the acetophenone hydrogenation catalyzed by Pd–[BMIm][PF_6] at 25 °C and 50 bar H_2. The spectra were taken in intervals of 20 min; the last one was recorded with a longer interval after 1000 min.

preferentially, but after 300 min the concentration of PE became higher than the concentration of AP, the rate of formation for cyclohexanol (CE) suddenly increased and the PE concentration stagnated and then started to drop. Thus, when using Rh–[BMIm][PF_6], the reaction has to be performed with low conversions under these conditions, if the goal is to optimize selectivity toward PE. Pd on the other hand did only create traces of by-products, with monotonic increase over the time and no apparent dependence on the concentration of other species. Thus, high conversion with high selectivity to PE can be achieved using this catalyst under the given conditions. The *in situ* ATR-IR experiments also allowed a more detailed analysis of the reaction progress regarding the selectivity to PE. The correlation between conversion and selectivity for Pd–[BMIm][PF_6] and Rh–[BMIm][PF_6] under different conditions is depicted in Fig. 5. Pd–[BMIm][PF_6] exhibited a high selectivity of more than 90% during the whole reaction, both at room temperature and at 40 °C. Complete conversions could be reached in all cases. On the other hand, Rh–[BMIm][PF_6] showed a continuous drop in selectivity under the same conditions (room temperature and 50 bar) but a much slower reaction progress. The experiment in this case was stopped after 15 h. Using a higher temperature of 80 °C accelerated the reaction considerably, but the selectivity dropped extremely fast after reaching approximately 45% conversion, when the formation of side products increased. This finding is consistent with the results of the hydrogenation reactions summarized in Section 3.2.

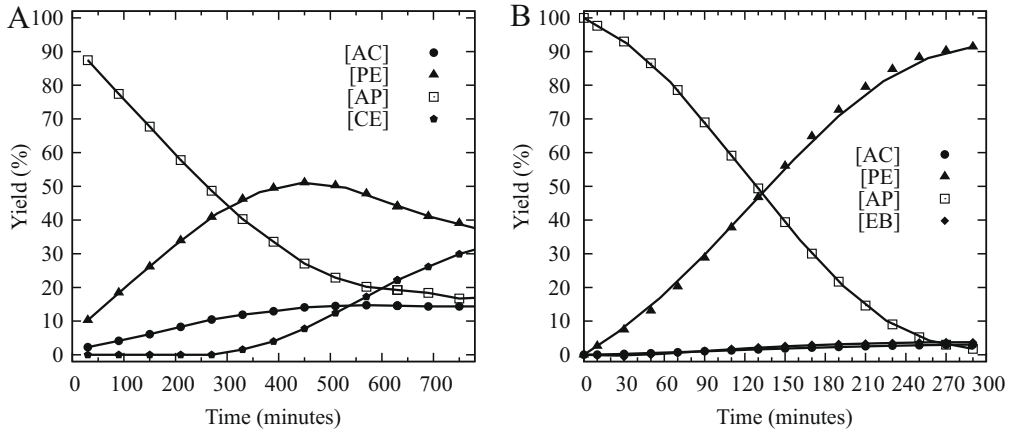

Fig. 4. Comparison of the reaction kinetics for the hydrogenation of acetophenone: (A) Rh–[BMIm][PF_6] at 80 °C and 50 bar H_2, and (B) Pd–[BMIm][PF_6] at room temperature and 25 bar H_2.

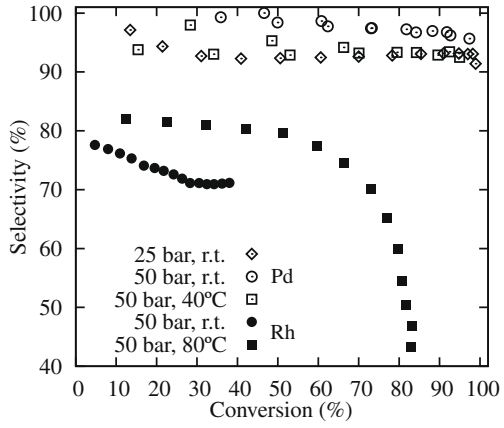

Fig. 5. Dependence of selectivity to 1-phenylethanol on conversion of acetophenone for Pd–[BMIm][PF_6] (open symbols) and Rh–[BMIm][PF_6] (black symbols) under various conditions.

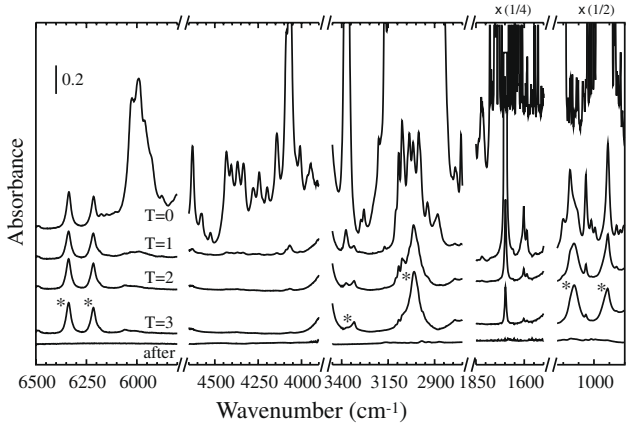

Fig. 6. *In situ* transmission IR spectra recorded during the supercritical CO_2 extraction of the hydrogenation products out of the ionic liquid phase. The top spectrum was recorded immediately after adding 100 bar of CO_2, while the other spectra were taken in intervals of 3 min during the continuous extraction process. The bands accentuated with an asterisk correspond to CO_2 at 100 bar.

3.4. Extraction of products by supercritical CO_2 and recycling of catalyst

In order to investigate the effectiveness of the product extraction by supercritical CO_2, *in situ* transmission IR spectra of the CO_2 phase were recorded during the extraction process. The results of this spectroscopic investigation are presented in Fig. 6. The first spectrum on top was recorded immediately after introducing 100 bar of CO_2 into the cell ($T = 0$). The product bands appeared instantly and reached saturation in several regions of the spectrum. Further spectra were recorded while a continuous flow of CO_2 was established. The following spectra show a fast decrease of the product bands. After 10 min, only the CO_2 bands were remaining in the recorded spectra (accentuated by asterisks). After releasing the pressure, no bands were observable in the gas phase. ATR-IR spectroscopy on the ionic liquid phase revealed a complete removal of the product and the reactant.

In order to investigate the catalytic activity upon recycling, six consecutive hydrogenation reactions and CO_2 extractions were performed. The results of this investigation are depicted in Fig. 7. ATR-IR spectra were recorded and analyzed according to the method described elsewhere [49], which provided time-resolved concentration profiles of each product. As Pd–[BMIm][PF_6] was employed as catalyst, only PE and EB were generated during the hydrogenation reactions. In the first experiment at room temperature and 50 bar, the selectivity for PE was comparably low, yielding

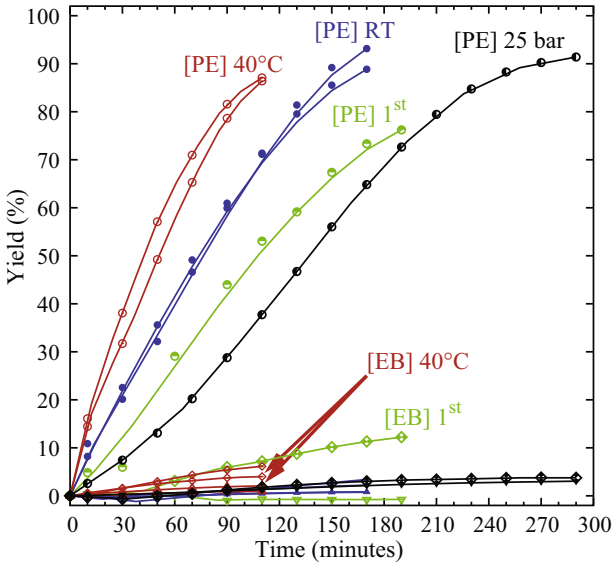

Fig. 7. Time-resolved concentration profiles of the hydrogenation products of acetophenone catalyzed by Pd–[BMIm][PF_6] during reuse experiments. Including the first run, three repetitions were performed at ambient temperature and 50 bar H_2, two repetitions at 40 °C and 50 bar, and one experiment at ambient temperature and 25 bar. For all experiments the same catalyst sample was employed.

more than 10% of EB as side product. This was due to the formation of HF in the aged catalyst, which will be explained in detail later. After the subsequent extraction process, the catalyst was however regenerated and the reaction yielded more than 90% of PE under the same conditions. The experiment at room temperature and 50 bar of hydrogen was repeated. After that, two further experiments were performed at 40 °C and 50 bar. With this procedure, the activity of the reused catalyst could be investigated more thoroughly, as both reaction temperature conditions were employed twice and the results thereof could be directly compared. Regarding this, Fig. 7 shows no loss of activity in terms of neither reaction rate nor product yield or selectivity upon reuse of the catalyst. As expected, the reaction at 40 °C appears faster, but the yield of PE is slightly lower, as more EB is formed which however remained at yields below 5%. At the end, one experiment at room temperature with a lower pressure of 25 bar was performed. This reaction progressed slower, but the same conversion and selectivity as with the other experiments were achieved. Thus, no loss in activity or in selectivity was observed after six reaction/extraction cycles using the same catalyst sample in reuse.

4. Discussion

4.1. Morphology of the nanoparticles

The nanoparticles synthesized in $N(C_6H_{13})_4Br$ exhibit a regular spherical shape and a narrow size distribution (Fig. 1). The particle sizes of both metal nanoparticles are in good agreement with the results reported for similar preparations. Caló et al. synthesized Pd nanoparticles in butyl-substituted ammonium bromide and obtained particles with an average diameter of 3.3 nm as well as comparable size distribution and dispersion [35]. Rh nanoparticles synthesized by Cimpeanu et al. using the same ionic liquid as in our work yielded well-dispersed spherical particles with an average diameter of 2.3 nm [31]. Under identical conditions Rh obviously forms smaller particles than Pd in alkylammonium bromide salts. As these ionic liquids are solid at room temperature, the particle dispersion remains more homogeneous over elongated time than in cases where RTILs are used, as in the latter the nanoparticles are much more mobile and tend to concentrate at the bottom of the storage vial after several days.

Remarkable differences were observed in the nanoparticles synthesized in [BMIm][PF_6] and [BMIm][OTf]. The particle size distribution of Rh–[BMIm][PF_6] is relatively broad and the shape is rather polygonal than spherical. Compared to published reports of Rh nanoparticles in [BMIm][PF_6], the size in our case is significantly larger. Fonseca et al. synthesized particles with an average diameter of 2.3 nm employing a different synthetic route, using $RhCl_3 \cdot 3H_2O$ as precursor [51], but also with a slight tendency to agglomerate. The same precursor was used by Léger et al., who prepared Rh nanoparticles with a size around 4 nm [43]. In that case, the dispersion was also much higher and the particles were more spherically shaped. However, they used $NaBH_4$ as reducing agent, which probably led to a more controlled reduction and growth of the Rh particles. The choice of the precursor complex and the reductant (among many other parameters) seems to have a great impact on the morphology and size of the nanoparticles. $Rh(acac)_3$ was not reduced at all in our case when using [BMIm][PF_6] as ionic liquid, while it worked perfectly in $N(C_6H_{13})_4Br$. As we wanted to avoid chloride in our system, for being a potential catalyst poison and very difficult to remove by supercritical CO_2, $Rh(OAc)_3$ was employed. Also for the reduction of the metal, H_2 was preferred over metal hydrides. Emphasizing the "green" approach, the impurities should be easily removable by supercritical CO_2 extraction and no potentially interfering cations should be brought into the system. The Rh particles in our case still have potential for improvement regarding size and shape; optimizing other parameters, e.g. hydrogen pressure, temperature, or concentration, could lead to smaller size and better dispersion.

The Pd nanoparticles show a relatively strong trend toward agglomeration. Pd–[BMIm][OTf] formed needle-shaped structures, while Pd–[BMIm][PF_6] exhibited rather round-shaped particles. The electron diffraction patterns of both are almost identical and indicate the existence of face-centered cubic structures of Pd in the samples, corresponding well to reports published on similar nanoparticles [52,53]. Very similar star-like shaped inter-particle organizations as in our Pd–[BMIm][OTf] were observed by Favier et al. using [$PdCl_2$(cod)] as precursor in a comparably simple synthetic approach [54]. The anion of the ionic liquid also plays an important role, as due to electronic interaction with the metal surface the anions electrostatically stabilize the particles [55]. Fonseca et al. synthesized Ir nanoparticles in both [BMIm][PF_6] and [BMIm][OTf]. There, the different ionic liquids also led to significant differences in size and shape of the particles [40]. Cassol et al. obtained Pd–[BMIm][PF_6] of small size and high dispersion, however, employing a much more complex synthetic route with no direct synthesis inside [BMIm][PF_6] [36]. Other reports include the utilization of additional stabilizers, such as phenanthroline [42], or the use of solid support materials [46]. These approaches seem to yield smaller and higher dispersed nanoparticles, but as in our case the particle size itself does not seem to be the most influential parameter for the catalytic activity, the simple preparation without additional additives was not considered exigent for optimization. In our case, the smaller Pd nanoparticles in $N(C_6H_{13})_4Br$ showed virtually no catalytic activity, while the large-sized and apparently agglomerated Pd–[BMIm][OTf] and Pd–[BMIm][PF_6] prove to be active, selective and reusable catalysts.

4.2. Catalytic activity

The turnover frequencies (TOFs) listed in Tables 1 and 2 are conservative estimates, calculated based on the total metal content and not on the number of surface atoms. These TOFs indicate that Pd-[BMIm][PF_6] is significantly more active than Rh in the same ionic liquid, although the latter appears to have a higher surface area. This is strikingly different when comparing the two metals in $N(C_6H_{13})_4Br$, where this effect is reversed. It is obvious that different metals and different ionic liquids have very specific possibilities for electronic interaction, which influences not only their size and shape during synthesis, but also their activity and selectivity during catalytic reactions. This is also the case when comparing Pd–[BMIm][PF_6] and Pd–[BMIm][OTf]. Although the size of the agglomerated particles is comparable, the morphology is significantly different, and so is the catalytic activity and chemoselectivity under the same reaction conditions. However, at this stage of research it would be extremely difficult to rationalize these effects without being highly speculative.

The catalytic activity of the catalysts reported is in the range of reported results of other catalytic AP hydrogenations. For example, a TOF of 13.9 h^{-1} is reported for a titanium phosphonate-supported Pd catalyst [7] with comparable selectivity. Also other reported metals with high selectivity reach TOFs of the same magnitude, e.g. Ni with 10.7 h^{-1} [10] or Pt with 19 h^{-1} [56]. Regarding other reported Pd catalysts, an often occurring problem is the selectivity toward PE, as EB is a subsequent product readily formed at conversions above 80% [5,57]. This problem is reportedly circumvented by cooling to −20 °C [7] or partial poisoning of the catalyst by amine ligands [58]. It is possible that the strongly interacting ionic liquid acts as a catalyst poison in a similar way, thus inhibiting the subsequent hydrogenolysis. This poisoning effect would also explain the comparably low activity of Rh in our case,

Table 1
Results of the hydrogenation of acetophenone catalyzed by Pd nanoparticles suspended in different ionic liquids.

Entry (−)	Ionic liquid (−)	AP/Pd ratio[a] (−)	T (°C)	p (bar)	Time (h)	Conversion (%)	Selectivity[b] (%)	TOF[c] (h^{-1})
1	[BMIm][PF_6]	78	25	50	4	97.7	89.9	19.0
2[d]	[BMIm][PF_6]	84	25	50	3	87.6	85.2	24.4
3[e]	[BMIm][PF_6]	84	25	50	3	95.1	93.6	26.5
4	[BMIm][PF_6]	84	40	50	2	89.1	97.4	37.2
5	[BMIm][PF_6]	152	50	50	4	71.4	86.5	27.1
6	[BMIm][PF_6]	114	50	10	4	86.3	67.3	24.6
7	[BMIm][PF_6]	60	25	50	2	42.1	99.8	12.7
8	[$N(C_6H_{13})_4$]Br	272	25	50	4	0.8	40.1	0.5
9	[BMIm][OTf]	164	25	15	4	27.6	99.9	2.3
10	[BMIm][OTf]	177	25	50	4	32.6	99.9	2.9
11	[BMIm][OTf]	104	25	100	4	17.8	99.9	4.6
12	[BMIm][OTf]	147	60	50	4	96.6	98	7.1

[a] Molar ratio between substrate (AP) and the total amount of Pd in a given reaction.
[b] Selectivity toward 1-phenylethanol (PE).
[c] Turnover frequency [$mol_{product}$ ($mol_{Pd\ in\ catalyst}$ h)$^{-1}$].
[d] Aged catalyst after storage for 3 months.
[e] Aged catalyst regenerated by supercritical CO_2 extraction.

Table 2
Results of the hydrogenation of acetophenone catalyzed by Rh nanoparticles suspended in different ionic liquids.

Entry (−)	Ionic liquid (−)	AP/Rh ratio[a] (−)	T (°C)	p (bar)	Time (h)	Conversion (%)	Selectivity[b] (%)	TOF[c] (h^{-1})
1	[BMIm][PF_6]	155	25	10	6	41.4	69.5	10.7
2	[BMIm][PF_6]	155	25	50	12	97.6	43.9	12.6
3	[BMIm][PF_6]	47	25	50	4	77.8	48.5	9.2
4	[BMIm][PF_6]	22	25	50	4	98.6	41.3	5.5
5	[BMIm][PF_6]	155	40	10	4	25.7	47.7	9.9
6	[BMIm][PF_6]	155	40	50	4	34.3	65.0	13.3
7	[BMIm][PF_6]	77	40	50	4	39.5	89.2	7.6
8	[BMIm][PF_6]	155	40	100	6	86.3	51.1	22.3
9	[BMIm][PF_6]	155	80	10	6	73.6	56.9	19.0
10	[BMIm][PF_6]	155	80	50	6	72.3	37.6	18.6
11	[$N(C_6H_{13})_4$]Br	392	25	50	4	39.5	42.2	38.7

[a] Molar ratio between substrate (AP) and the total amount of Rh in a given reaction.
[b] Selectivity toward 1-phenylethanol (PE).
[c] Turnover frequency [$mol_{product}$ ($mol_{Rh\ in\ catalyst}$ h)$^{-1}$].

which normally is very active even at ambient temperature and pressure. The synthesis-based chloride content in [BMIm][PF_6] of less than 10 ppm cannot explain the difference in activity sufficiently. This is especially the case when comparing Rh–[BMIm][PF_6] and Pd–[BMIm][PF_6], as both contain the same ionic liquid and further contamination with halides was carefully avoided. One limitation of using metals in ionic liquids is also the diffusion of gases inside. In [BMIm][PF_6] at room temperature, the hydrogen solubility is 4.4 mmol/L at 5 bar, 44 mmol/L at 50 bar, and 890 mmol/L at 100 bar [59]. Under the conditions used in the present work, however, where a smaller volume of ionic liquid was present in the reactions compared to the substrate, this limitation did not significantly influence the activity of the catalysts.

4.3. Hydrolysis of PF_6^-

One of the synthesized catalysts, Pd–[BMIm][PF_6], underwent partial decomposition upon prolonged storage under non-dried air conditions. It was noted that after 3 months of storage, the vial containing the catalyst released a slight smell of halogen acid when opened. As shown in the catalytic results, this aged catalyst was still active, but yielded more of the undesired hydrogenolysis product EB, which is formed especially under acidic conditions during hydrogenations with Pd [60]. Rangits et al. investigated Pd and Pt species in [BMIm][PF_6] and found in NMR experiments that the PF_6^- anion undergoes partial hydrolysis in the presence of small amounts of water. The hydrolysis reaction, which produces HF, obviously also takes place in the absence of noble metals, but their presence accelerates the formation of the acid [61,62]. As mentioned before, this effect led in our experiments to increased acid-promoted formation of EB. However, as the reuse experiments show, a single extraction step by supercritical CO_2 prior to the hydrogenation reaction is able to remove HF and regenerate the catalyst to its full initial activity. After this, careful storage under dry conditions should prevent further hydrolysis.

The formation of HF and the consequences on the selectivity were only observed with Pd–[BMIm][PF_6]. Using [BMIm][OTf] as ionic liquid prevents the formation of HF completely, as it is not prone to such a hydrolysis reaction.

4.4. Reaction kinetics

The reaction kinetics investigated by means of *in situ* IR spectroscopy and subsequent data analysis showed the same characteristic features as reported for similar systems in the literature. Bergault et al. reported a thorough kinetic study on the liquid-phase hydrogenation of acetophenone catalyzed by Rh on carbon [63]. Although the overall reaction in their report is faster than in our case, the relative rates of formation of the different products are very similar. Apparently [BMIm][PF_6] is not significantly influencing the product distribution by its interaction with Rh, and the selectivity is not altered by this effect. [BMIm][PF_6] rather has a slowing effect for all competitive reactions, either by coordinative-

ly blocking active sites or by adding a diffusion barrier around the metal particle. However, it is possible that with further optimization of other reaction parameters, such as pressure and temperature, better selectivity may be achieved. Also different ionic liquids, which interact distinctively with specific reaction products, might help to optimize the selectivity.

Regarding Pd–[BMIm][PF_6], the reaction kinetics slightly differ from published results on other Pd-catalyzed AP hydrogenation systems. As mentioned before, in many reports the subsequent hydrogenolysis to EB increases significantly at higher conversions. At room temperature and without the addition of a base, the maximum yield of around 80% was reported, before rapid hydrogenolysis decreased the PE concentration [7,57]. A similarly high selectivity as in our system was achieved by Drelinkiewicza et al. employing basic polymer supports, e.g. polypyrrole [5]. There, PE concentrations of over 90% were measured before the subsequent hydrogenolysis reaction started. It is thus possible that [BMIm]-[PF_6] has a similar effect on the Pd-catalyzed AP hydrogenation as a basic polymer support, either by similar interactions with Pd or by hindering the formation of EB due to the basicity.

4.5. Recycle experiments

The recycle experiments performed with Pd–[BMIm][PF_6] showed no noticeable deactivation of the catalyst after six cycles. Both conversion and selectivity did not decrease; a behavior which was also reported by Fonseca et al. after repeatedly recycling Ir nanoparticles in [BMIm][PF_6], while without the ionic liquid the activity decreased [64]. Also the efficient product extraction by supercritical CO_2 appears to offer advantages compared to filtration techniques, because the catalyst remains inside the reactor all the time and thus no catalyst material is lost during the separation step. This is only possible because both the ionic liquid and the particles themselves are practically insoluble in CO_2. Apart from that, nanoparticles immobilized in ionic liquids do not suffer from blockage of pores or similar phenomena which often occur in solid-supported metal catalysts, especially in recycle. Furthermore, the stabilizing effect of the ionic liquids makes reductive activation of the catalysts redundant, a preceding step often required when using other noble metal catalysts.

5. Conclusions

The combination of ionic liquids and supercritical CO_2 allowed the design of a "green" reaction pathway consisting of a simple catalyst synthesis and efficient product separation. Pd- and Rh-nanoparticles were successfully synthesized by the reduction of the corresponding metal precursors in different ionic liquids followed by the removal of the metal ligands by supercritical carbon dioxide extraction. Among the tested catalysts, Pd–[BMIm][PF_6] showed the best performance. The catalyst showed no deactivation in repetitive reaction cycles. The slight loss in activity observed in the first reaction cycle could be eliminated by subsequent supercritical CO_2 extraction and traced to some hydrolysis of the PF_6^- anions. *In situ* IR spectroscopy was employed to study the kinetics of the complex reaction pathway and to monitor the product extraction by supercritical CO_2. The combination of *in situ* synthesis of noble metal nanoparticles in suitable ionic liquids with supercritical CO_2 extraction should offer a great potential for further developments in heterogeneous catalysis. Not only the "green" aspects (solventless conditions and simple product extraction) of such processes are striking, but also the molecular interactions of ionic liquids with catalytic nanoparticles appear interesting for tuning the catalyst properties. Nevertheless, today these interactions are not yet sufficiently understood for a rational design of such catalyst systems.

Acknowledgments

We thank Dr. Frank Krumeich for the electron microscopy investigations performed at the electron microscopy center at ETH Zurich (EMEZ), and the Bundesamt für Energie (BFE) for financial support of this work.

Appendix A. Supplementary data

Supplementary data associated with this article can be found, in the online version, at doi:10.1016/j.jcat.2009.10.006.

References

[1] P. Maki-Arvela, J. Hajek, T. Salmi, D.Y. Murzin, Appl. Catal. A 292 (2005) 1.
[2] L.P. Christensen, M. Edelenbos, S. Kreutzmann, in: R.G. Berger (Ed.), Flavours and Fragrances–Chemistry Bioprocessing and Sustainability, Springer, New York, 2007.
[3] N.M. Bertero, C.R. Apesteguía, A.J. Marchi, Appl. Catal. A 349 (2008) 100.
[4] C.S. Chen, H.W. Chen, W.H. Cheng, Appl. Catal. A 248 (2003) 117.
[5] A. Drelinkiewicza, A. Waksmundzka, W. Makowski, J.W. Sobczak, A. Krol, A. Zieba, Catal. Lett. 94 (2004) 143.
[6] F. Gao, A.D. Allian, H. Zhang, S. Cheng, M. Garland, J. Catal. 241 (2006) 189.
[7] Y.L. Ji, X.B. Ma, X.J. Wu, Q. Wang, Appl. Catal. A 332 (2007) 247.
[8] S.D. Lin, D.K. Sanders, M. Albert Vannice, Appl. Catal. A 113 (1994) 59.
[9] F. Zaccheria, N. Ravasio, R. Psaro, A. Fusi, Tetrahedron Lett 46 (2005) 3695.
[10] R.V. Malyala, C.V. Rode, M. Arai, S.G. Hegde, R.V. Chaudhari, Appl. Catal. A 193 (2000) 71.
[11] P. Claus, Top. Catal. 5 (1998) 51.
[12] K. Anderson, P. Goodrich, C. Hardacre, D.W. Rooney, Catal. Appl. (2003) 272.
[13] J.F. Brennecke, E.J. Maginn, AIChE J. 47 (2001) 2384.
[14] M.J. Earle, J. Esperanca, M.A. Gilea, J.N.C. Lopes, L.P.N. Rebelo, J.W. Magee, K.R. Seddon, J.A. Widegren, Nature 439 (2006) 831.
[15] Y. Gu, G. Li, Adv. Synth. Catal. 351 (2009) 817.
[16] M. Haumann, A. Riisager, Chem. Rev. 108 (2008) 1474.
[17] N. Jain, A. Kumar, S. Chauhan, S.M.S. Chauhan, Tetrahedron 61 (2005) 1015.
[18] C.P. Mehnert, R.A. Cook, N.C. Dispenziere, M.J. Afeworki, Am. Chem. Soc. 124 (2002) 12932.
[19] R. Sheldon, Chem. Commun. (2001) 2399.
[20] T. Welton, Chem. Rev. 99 (1999) 2071.
[21] T. Welton, Coord. Chem. Rev. 248 (2004) 2459.
[22] T. Welton, P.J. Smith, Adv. Organomet. Chem. 51 (2004) 251.
[23] A. Ahosseini, W. Ren, A.M. Scurto, Chim. Oggi 25 (2007) 40.
[24] A. Ahosseini, W. Ren, A.M. Scurto, Ind. Eng. Chem. Res. 48 (2009) 4254.
[25] J.-M. Andanson, F. Jutz, A. Baiker, J. Phys. Chem. B 113 (2009) 10249.
[26] U. Hintermair, G.Y. Zhao, C.C. Santini, M.J. Muldoon, D.J. Cole-Hamilton, Chem. Commun. (2007) 1462.
[27] S.G. Kazarian, B.J. Briscoe, T. Welton, Chem. Commun. (2000) 2047.
[28] S. Keskin, D. Kayrak-Talay, U. Akman, O. Hortacsu, J. Supercrit. Fluids 43 (2007) 150.
[29] M. Roth, J. Chromatogr. A 1216 (2009) 1861.
[30] M. Solinas, A. Pfaltz, P.G. Cozzi, W. Leitner, J. Am. Chem. Soc. 126 (2004) 16142.
[31] V. Cimpeanu, M. Kocevar, V.I. Parvulescu, W. Leitner, Angew. Chem. Int. Ed. 48 (2009) 1085.
[32] S.G. Kazarian, N. Sakellarios, C.M. Gordon, Chem. Commun. (2002) 1314.
[33] A.M. Scurto, E. Newton, R.R. Weikel, L. Draucker, J. Hallett, C.L. Liotta, W. Leitner, C.A. Eckert, Ind. Eng. Chem. Res. 47 (2008) 493.
[34] D. Tomida, A. Kumagai, K. Qiao, C. Yokoyama, J. Chem. Eng. Data 52 (2007) 1638.
[35] V. Calo, A. Nacci, A. Monopoli, S. Laera, N. Cioffi, J. Org. Chem. 68 (2003) 2929.
[36] C.C. Cassol, A.P. Umpierre, G. Machado, S.I. Wolke, J. Dupont, J. Am. Chem. Soc. 127 (2005) 3298.
[37] J.H. Cha, K.S. Kim, H. Lee, Korean J. Chem. Eng. 26 (2009) 760.
[38] J. Dupont, G.S. Fonseca, A.P. Umpierre, P.F.P. Fichtner, S.R. Teixeira, J. Am. Chem. Soc. 124 (2002) 4228.
[39] G.S. Fonseca, J.B. Domingos, F. Nome, J. Dupont, J. Mol. Catal. A: Chem. 248 (2006) 10.
[40] G.S. Fonseca, G. Machado, S.R. Teixeira, G.H. Fecher, J. Morais, M.C.M. Alves, J. Dupont, J. Colloid Interface Sci. 301 (2006) 193.
[41] B. Ganchegui, S. Bouquillon, F. Henin, J. Muzart, Tetrahedron Lett. 43 (2002) 6641.
[42] J. Huang, T. Jiang, B.X. Han, H.X. Gao, Y.H. Chang, G.Y. Zhao, W.Z. Wu, Chem. Commun. (2003) 1654.
[43] B. Leger, A. Denicourt-Nowicki, H. Olivier-Bourbigou, A. Roucoux, ChemSusChem 1 (2008) 984.
[44] P. Migowski, J. Dupont, Chem. Eur. J. 13 (2007) 32.
[45] M.H.G. Prechtl, M. Scariot, J.D. Scholten, G. Machado, S.R. Teixeira, J. Dupont, Inorg. Chem. 47 (2008) 8995.

[46] M. Ruta, G. Laurenczy, P.J. Dyson, L. Kiwi-Minsker, J. Phys. Chem. C 112 (2008) 17814.
[47] C.W. Scheeren, J.B. Domingos, G. Machado, J. Dupont, J. Phys. Chem. C 112 (2008) 16463.
[48] P. Singh, K. Kumari, A. Katyal, R. Kalra, R. Chandra, Spectrochim. Acta Part A 73 (2009) 218.
[49] J.-M. Andanson, F. Jutz, A. Baiker, submitted for publication.
[50] M.S. Schneider, J.-D. Grunwaldt, T. Bürgi, A. Baiker, Rev. Sci. Instrum. 74 (2003) 4121.
[51] G.S. Fonseca, A.P. Umpierre, P.F.P. Fichtner, S.R. Teixeira, J. Dupont, Chem. Eur. J. 9 (2003) 3263.
[52] P.F. Ho, K.M. Chi, Nanotechnology 15 (2004) 1059.
[53] C.C. Wang, D.H. Chen, T.C. Huang, Colloids Surf. A 189 (2001) 145.
[54] I. Favier, E. Teuma, M. Gomez, CR Chim. 12 (2009) 533.
[55] S. Ozkar, R.G. Finke, J. Am. Chem. Soc. 124 (2002) 5796.
[56] H.P. Liu, G.Z. Lu, Y. Guo, Y.Q. Wang, Y.L. Guo, Catal. Commun. 10 (2009) 1324.
[57] M.A. Aramendia, V. Borau, J.F. Gomez, A. Herrera, C. Jimenez, J.M. Marinas, J. Catal. 140 (1993) 335.
[58] K. Hattori, H. Sajiki, K. Hirota, Tetrahedron 57 (2001) 4817.
[59] J.P. Mikkola, J. Warna, P. Virtanen, T. Salmi, Ind. Eng. Chem. Res. 46 (2007) 3932.
[60] R.W. Meschke, W.H. Hartung, J. Org. Chem. 25 (1960) 137.
[61] G. Rangits, L. Kollar, J. Mol. Catal. A: Chem. 242 (2005) 156.
[62] G. Rangits, G. Petocz, Z. Berente, L. Kollar, Inorg. Chim. Acta 353 (2003) 301.
[63] I. Bergault, P. Fouilloux, C. Joly-Vuillemin, H. Delmas, J. Catal. 175 (1998) 328.
[64] G.S. Fonseca, J.D. Scholten, J. Dupont, Synlett (2004) 1525.